

1  
2  
3  
4  
5  
6  
7  
8  
9  
10  
11  
12  
13  
14  
15  
16  
17  
18  
19  
20  
21  
22

**Architecture of the ring formed by the tubulin  
homologue FtsZ in bacterial cell division**

Piotr Szwedziak <sup>1, \*</sup>, Qing Wang <sup>1, \*</sup>, Tanmay AM Bharat <sup>1</sup>, Matthew Tsim <sup>1</sup>, Jan  
Löwe <sup>1, †</sup>

<sup>1</sup> MRC Laboratory of Molecular Biology, Structural Studies Division, Francis Crick  
Avenue, Cambridge, CB2 0QH, United Kingdom

\* PS and QW contributed equally to this work.

† Corresponding author: Jan Löwe, MRC Laboratory of Molecular Biology, Francis  
Crick Avenue, Cambridge CB2 0QH, UK, email: [jyl@mrc-lmb.cam.ac.uk](mailto:jyl@mrc-lmb.cam.ac.uk), phone:  
+44 1223 267064

Keywords: FtsZ, FtsA, divisome, bacterial cell division, cytokinesis

## 23 **Summary:**

24 Membrane constriction is a prerequisite for cell division. The most common  
25 membrane constriction system in prokaryotes is based on the tubulin homologue FtsZ,  
26 whose filaments in *E. coli* are anchored to the membrane by FtsA and enable  
27 formation of the Z ring and divisome. The precise architecture of the FtsZ ring has  
28 remained enigmatic. Here, we report three-dimensional arrangements of FtsZ and  
29 FtsA filaments in *C. crescentus* and *E. coli* cells and inside constricting liposomes by  
30 means of electron cryomicroscopy and cryotomography. *In vivo* and *in vitro*, the Z-  
31 ring is composed of a small, single-layered band of filaments parallel to the  
32 membrane, creating a continuous ring through lateral filament contacts. Visualisation  
33 of the *in vitro* reconstituted constrictions as well as a complete tracing of the helical  
34 paths of the filaments with a molecular model favour a mechanism of FtsZ-based  
35 membrane constriction that is likely to be accompanied by filament siding.

## 38 **Highlights:**

- 39 • Filaments of the Z ring in *C. crescentus*, *E. coli* and inside liposomes revealed  
40 by tomography
- 41 • Spontaneous, nucleotide-independent constriction of FtsAZ-loaded liposomes
- 42 • Architecture of the FtsZ ring is similar *in vivo* and *in vitro*
- 43 • Overlapping filaments in closed ring of FtsZ might slide, leading to new  
44 mechanism

## 46 **Introduction:**

47 Membrane dynamics during cytokinesis are some of the most fundamental processes  
48 in biology, yet poorly understood at the molecular and mechanistic level. During  
49 prokaryotic cell division the cell membrane and the cell envelope constrict, eventually  
50 leading to cell separation. In most bacteria and archaea this is guided by a ring  
51 structure containing the bacterial tubulin homologue FtsZ protein (Bi and Lutkenhaus,  
52 1991; Löwe and Amos, 1998), which polymerises in a GTP-dependent manner  
53 (Mukherjee and Lutkenhaus, 1994). During constriction, the FtsZ-ring decreases in  
54 diameter through an unknown mechanism. The C-terminal tail of FtsZ links it to other  
55 components of the divisome, an ensemble of many proteins that facilitates essential  
56 functions during the cell division process, most importantly remodelling of the cell  
57 envelope. Components of the divisome engage in cell wall synthesis (PBPs),  
58 synchronisation with chromosome dimer resolution (FtsK), lipid II cell wall precursor  
59 flipping (FtsW or MurJ) and many components currently have no known function  
60 (reviews: (Adams and Errington, 2009; Lutkenhaus et al., 2012)).

61 In *Escherichia coli*, binding of the FtsZ tail to ZipA and possibly more importantly to  
62 FtsA anchors the FtsZ-ring to the membrane (Pichoff and Lutkenhaus, 2007). FtsA is  
63 a bacterial actin-like protein that forms domain-swapped, canonical actin-like  
64 protofilaments that are membrane associated through FtsA's C-terminal amphipathic  
65 helix (Pichoff and Lutkenhaus, 2005; Szwedziak et al., 2012; van den Ent and Löwe,  
66 2000). Several cellular regulatory processes influence the onset and progression of  
67 cell division through mechanisms that directly act on FtsZ. For example, SulA is  
68 induced during the SOS stress response and sequesters monomers, stopping FtsZ  
69 polymerisation (Chen et al., 2012). In *E. coli*, both nucleoid occlusion and the  
70 oscillating, pole-protecting MinCDE system contain components that inhibit FtsZ  
71 function within the ring directly (Bernhardt and de Boer, 2005; Dajkovic et al., 2008).

72 Although progress has been exhilarating over that past 20 years or so, some of the  
73 most fundamental questions still remain: what happens during FtsZ-ring constriction?  
74 How are the filaments arranged in the ring? What drives constriction?

75 Many different models have been proposed for the mechanism of FtsZ-based  
76 constriction (reviewed in (Erickson, 2009; Erickson et al., 2010)). Essentially, three  
77 different approaches have been taken to validate the models: *in vivo* imaging of FtsZ  
78 constrictions using fluorescently labelled proteins. Electron cryotomography of frozen  
79 hydrated cells without labelling and thirdly *in vitro* reconstitution experiments with  
80 pure, fluorescently labelled proteins. The most recent results emanating from those  
81 studies are that the rings appear to show strong fluorescence intensity variations that  
82 may suggest that the FtsZ ring is discontinuous (Holden et al., 2014). Equally,  
83 tomography data has been interpreted to show scattered, individual FtsZ filaments  
84 some precise distance away from the membrane (Li et al., 2007). Reconstitution  
85 experiments with FtsZ and FtsA showed dynamic behaviour and liposome  
86 constrictions (Loose and Mitchison, 2014; Osawa and Erickson, 2013). However,  
87 obtaining detailed, molecular and mechanistic information regarding the FtsZ ring,  
88 particularly the arrangement of individual filaments and subunits within a constricting  
89 Z- ring, has remained a formidable challenge.

90 Here, we obtained high-resolution images of the FtsZ ring in *Caulobacter crescentus*  
91 and *Escherichia coli* by means of electron cryotomography. Furthermore, we  
92 reconstituted a minimal constriction force-generating system from purified  
93 components *in vitro*, encapsulating *Thermotoga maritima* FtsA (TmFtsA) and FtsZ  
94 (TmFtsZ) in liposomes of sizes corresponding to those of a bacterial cell. We  
95 produced images and three-dimensional maps of filaments arranging themselves into  
96 ring structures around the liposome perimeters that coincided with constriction sites.

97 The observed FtsZ ring architectures in *C. crescentus* and *E. coli* cells and in  
98 liposomes favour a mechanism of FtsZ-based cell membrane constriction that is  
99 accompanied by filament sliding, as was proposed previously (Lan et al., 2009).

**Results:****Single-layered and continuous FtsZ ring in unmodified *C. crescentus* cells.**

We started out by visualising division sites in an unmodified *C. crescentus* strain (NA1000/CB15N) because the thin *Caulobacter* cells are most suitable for electron cryotomography. When a log-phase culture was plunge-frozen and imaged, many dividing cells could be found. At the division sites, a series of dots arranged in a single line were found (Figure 1A, top). Careful analysis of cellular tomograms (Movie M1 and Figure 1A, bottom) revealed that the dots were in fact 2D projections of filamentous structures encircling the cell and likely forming a continuous ring, disrupted in the images at the top and bottom by the missing wedge of the tomography method. The filaments were at a distance of  $15 \pm 2$  nm from the inner membrane (Figure 1B) as previously reported (Li et al., 2007). The long-standing problem of the missing wedge in electron tomography caused by our current inability to tilt the specimen much beyond  $65^\circ$  (Figure 1A, bottom, white triangle, see also Figure 1—figure supplement 1 for more details on the missing wedge problem related to this study) makes it impossible to follow features all the way around the cell's perimeter. It is important to note, however, that the protein filaments are visible and un-interrupted everywhere the missing wedge allows it, as can be gauged from the disappearance of the cell membrane and envelope (Figure 1A & B). We could detect the filamentous rings in 20 out of 28 dividing cells after tomography. Of the 8 without obvious filamentous structures, in 3 the division had progressed too far and 5 were of poor quality because of the cell's orientation with respect to the tilt axis (Figure 1—figure supplement 1). Hence, the finding of complete rings is supported by the fact that perfect coincidence of any hypothetical gaps in constricting rings with the

missing wedges in all of the analysed tomograms, found after all in entirely random orientations, would be remarkably implausible.

**Identical FtsZ ring architecture in unmodified *E. coli*.**

To investigate the generality of these findings, we imaged unmodified *E. coli* B/r H266 cells, which we chose because of their thinness (Woldringh, 1976). Although the *E. coli* cells were thicker than *C. crescentus*, we found the wild-type filaments still discernible, most obviously when imaged along the long axis of cells (Figure 1C and Figure 1—figure supplement 2, especially B and D; Movie M2), and these were 16 nm away from the IM. Based on these observations we concluded that *E. coli* Z-rings were, like in *C. crescentus*, probably continuous and consisted of single-layered bands that are 5-10 filaments wide.

In order to investigate if the filaments imaged in wild-type cells so far contained FtsZ protein, we over-expressed FtsZ(D212A), a mutant protein that hydrolyses GTP much more slowly (Redick et al., 2005) in *E. coli* B/r H266 cells. When over-expressed to 2.5 fold total FtsZ (Figure 1D), the protein formed a wide single layer of filaments at the division site (Figure 1E, see also Movie M3 and Figure 1—figure supplement 3), very similar to the bands seen in unmodified cells, but wider and containing more filaments as would be expected because there is now more FtsZ protein in the cell and filament dynamics have been reduced because of the GTPase-reducing mutation D212A. Figure 1F (Figure 1—figure supplement 3A-C) provides a view rotated by 90°, showing again that the filamentous ring was located approximately 16 nm away from the inner membrane (IM). The band of filaments most likely consisted of doublets of individual protofilaments, as is indicated in Figure 1G, which shows a cell with higher expression level (Figure 1—figure supplement 3A-C). The filaments were

on average 6.8 nm apart ( $n = 17$ , distance between centres of adjacent filaments within a doublet, Figure 1G, lower). It is currently not known what lateral interactions between FtsZ filaments cause this arrangement or if it is facilitated by other proteins.

**The filaments observed in the tomograms are FtsZ.**

Because no specific label for electron cryotomography currently exists that works in *E. coli*, we decided to further confirm the identity of the filaments as being composed of FtsZ by systematic perturbations of the system in four (a-d) separate experiments with subsequent imaging by electron cryotomography (Figure 1—figure supplement 5, Supplementary File 1A & 1B). (a) Introducing extra amino acids into the flexible linker (Buske and Levin, 2013; Gardner et al., 2013) within FtsZ that separates the globular N-terminal domain of FtsZ from the small C-terminal helix that binds FtsZ's membrane anchor, FtsA (Ma and Margolin, 1999; Szwedziak et al., 2012), increased the distance between the FtsZ ring and the IM from 16 nm to a somewhat variable 16 - 21 nm (Figure 1H and Figure 1—figure supplement 4A-C). (b) Removing the C-terminal FtsA-interacting helix and replacing it with a membrane-targeting sequence (mts) from MinD protein (Hu and Lutkenhaus, 2003) shortened the distance from the IM to 10 nm. No constrictions of the cells were observed (Figure 1I and Figure 1—figure supplement 4D). Therefore, despite it having been used in earlier studies (Loose and Mitchison, 2014; Osawa et al., 2008; Osawa et al., 2009; Osawa and Erickson, 2011), we agree with previous findings (Osawa et al., 2008) that this construct is non-functional *in vivo* and we did not include it in our subsequent *in vitro* investigations below. (c) Removing the C-terminal FtsA-interacting helix from FtsZ detached the filaments from the membrane, making them appear throughout the cytoplasm (Figure 1J and Figure 1—figure supplement 4E). (d) Finally, removing most amino acids between the C-terminal FtsA-interacting helix and the globular

body of FtsZ caused a minicell phenotype. Because of their size, minicells produce tomograms of higher quality and it was possible to determine the longitudinal subunit repeat of the filaments to be around 4 nm, very close to the expected value of 4.2 nm for FtsZ (Figure 1K & L and Figure 1—figure supplement 4G) (Erickson et al., 1996). We conclude that the filament localisations reacted to our perturbations as expected for FtsZ and the subunit repeat was the same as for all known FtsZ protofilaments. The minicell tomogram (Figure 1K) is another indication that the filaments most likely encircle entire cells.

### **Extra septa generated by additional FtsZ and FtsA function in cell separation.**

Encouraged by reports that simultaneous overexpression of FtsZ and its membrane anchor FtsA led to additional division sites (Begg et al., 1998), we imaged *E. coli* cells in which extra FtsZ(D212A) and FtsA were produced from a bicistronic expression vector, by electron cryotomography (Figure 2A-E). Providing just these two proteins in excess (2 to 4-fold total vs. WT) produced a severe phenotype with many extra constrictions visible (Figure 2A & B). Since in these cells the normal FtsZ to FtsA ratio had been altered to be close to 1:1, from normally 5 FtsZ : 1 FtsA (Rueda et al., 2003), FtsA filaments became visible at the constricting division sites (Figure 2C-E). Actin-like FtsA binds to the membrane directly via its C-terminal amphipathic helix and polymerises into canonical actin-like protofilaments (Lara et al., 2005; Szwedziak et al., 2012). In this way, an artificially strong 'FtsA ring' became apparent, indicating that FtsA is located between the IM and FtsZ, being 8 nm away from both (Figure 2D & E).

We then demonstrated that the FtsZ(D212A) and FtsA-overexpressing *E. coli* cells we had imaged at high resolution with electron cryotomography were dividing and

separating, despite looking quite distorted. For this we employed structured illumination microscopy (SIM) on live cells (Figure 2F). The cells showed a strong minicell phenotype, while performing many cell divisions randomly distributed along the cell length. This indicated to us that the extra constrictions and division sites were functional in the sense that they led to complete cell separation (abscission).

We concluded that the ability to produce extra constriction sites and divisions by just providing more FtsZ and FtsA indicates that these two proteins may be central components of the IM constriction force generator that is localised within the inner division apparatus (Rico et al., 2013) and that it may be possible to reconstitute membrane constriction with just the two of them. Indeed, this has recently been reported and has been imaged at low resolution using fluorescence microscopy (Osawa et al., 2008; Osawa and Erickson, 2013), although not providing any molecular insights.

#### **Reconstituting liposome constrictions *in vitro* using *T. maritima* FtsA and FtsZ.**

So we then used purified FtsZ and FtsA proteins for *in vitro* reconstitution experiments, in order to observe constriction. We avoided fluorescently tagged proteins as they have been shown to introduce artefacts (Margolin, 2012). We therefore used completely unmodified TmFtsZ and TmFtsA proteins from *Thermotoga maritima*, both of which are easy to obtain and handle and have crystal structures available (Oliva et al., 2004; van den Ent and Löwe, 2000). It should be noted that extra care had to be taken in order to obtain proteins that did not have their disordered but important C-terminal tails cleaved during purification. Just to confirm that TmFtsZ and TmFtsA formed structures similar to the *E. coli* counterparts *in vivo*, we overexpressed TmFtsZ and TmFtsA in *E. coli* and imaged the sample by electron

cryotomography (Figure 2G). Minicells were formed and at constriction sites they contained filaments that closely resembled the filament arrangement observed here for *E. coli* FtsA and FtsZ overexpression in *E. coli* (Figure 2C). The distance of TmFtsZ to the IM was shorter at 12 nm; this was expected because the linker between the very C-terminal TmFtsA-interacting helix and the body of TmFtsZ is much shorter, measuring around 9 amino acids. Minicell formation might indicate that TmFtsA and TmFtsZ interacted with the *E. coli* cell division machinery or even supported membrane constriction on their own, but we did not investigate this further.

#### **FtsA and FtsZ form spirals on a flat lipid surface.**

When added onto a flat lipid monolayer, TmFtsZ and TmFtsA formed striking spirals (Figure 3A). The filaments forming the spirals tended to form weak doublets and in the centre of the spirals white material was visible that may have been lipid that had been pushed up by the spiral constricting, possibly via a sliding filament mechanism as has previously been observed for FtsZ alone by AFM (Mingorance et al., 2005). Intriguingly, much larger dynamic chiral spirals of polar FtsA and FtsZ filaments have recently been reported on supported lipid bilayers (Loose and Mitchison, 2014) but the exact relationship with our observation is currently unclear as treadmilling and no constriction was observed on the supported bilayers.

#### **FtsA and FtsZ polymers together generate negative curvature on liposome surfaces.**

Since the FtsZ ring *in vivo* does not act on flat membranes, we then switched to liposomes formed from *E. coli* lipid extract. First, TmFtsZ and TmFtsA were added to pre-formed liposomes so that the proteins remained on the outside (Figure 3B and Figure 3—figure supplement 1A). Reactions containing liposomes and proteins as

indicated were vitrified and imaged by conventional 2D transmission electron cryomicroscopy. When no protein was added, the liposomes appeared as almost perfect circles (spheres in projection) and the bilayers were clearly visible as a double line, 5 nm apart (Figure 3B, top, Figure 3—figure supplement 2D). The addition of TmFtsA alone led to formation of an additional layer, probably consisting of only partly polymerised protein, and no strong deformations were observed. TmFtsZ alone did not cause deformations or generation of an additional layer (Figure 3—figure supplement 2B). But when both TmFtsA and TmFtsZ were added, two extra layers, in addition to the liposome bilayer, became visible (Figure 3B). Particularly in the presence of nucleotide, strong negative curvature was induced, leading to deformations of the liposomes (Figure 3—figure supplement 1A). As was suggested previously, the co-polymerisation of FtsZ and FtsA will lead to bending and curvature because the subunit repeat lengths of FtsZ and FtsA are roughly 4 and 5 nm, respectively (Figure 3—figure supplement 1B and Figure 3—figure supplement 2A) (Szwedziak et al., 2012). We propose that the subunit repeat mismatch causes some deformations from the outside of the liposomes, especially when FtsZ polymerisation-inducing GMPCPP is present so that long filaments are formed that will exert more mechanical force.

### **Incorporating FtsA and FtsZ on the inside of liposomes leads to spontaneous constrictions.**

Since TmFtsZ and TmFtsA induce negative membrane curvature, we concluded that in order to reconstitute the actions of these proteins correctly, we needed to incorporate them on the inside of liposomes. For this, CHAPS detergent-solubilised *E. coli* lipid extract was mixed with the proteins at high concentrations and then diluted many-fold. Lowering of the detergent concentration by dilution led to

spontaneous liposome formation with most of the proteins on the inside. We demonstrated with a time-lapse experiment that liposomes did not form around pre-existing FtsZ scaffolds since we observed that most liposomes were initially perfectly spherical and that they deformed over a 30-minute period, after which most of them were heavily misshapen (Figure 3—figure supplement 2C, E).

The liposomes were then analysed by transmission electron cryomicroscopy. Amazingly, when both TmFtsZ and TmFtsA were included on the inside of liposomes, clear constriction sites appeared and these occurred only when supported by filaments (Figure 3C-G). The liposomes were around 300 nm in diameter, similar to that of a small bacterial cell. The protein filaments were arranged into three distinct structures: arcs that were mostly single filaments, presumably formed by the copolymerisation of TmFtsZ and TmFtsA, showing the characteristic curvature caused by the repeat mismatch (Szwedziak et al., 2012); spirals with decreasing curvature that appeared in perfectly spherical areas of the liposomes; and rings of filaments, appearing as bands in projection, formed around liposome constriction sites, with varying diameters. It is very important to note that constrictions only appeared where there were rings of filaments. Filaments within the liposomes had very different curvatures, for example in Figure 3D, filaments seemed to go round the liposome at a very large diameter, compared to the ones in the constriction zone further to the left.

When the constriction sites were imaged at higher magnification, it became possible to discern the TmFtsA and TmFtsZ filaments end-on (Figure 3H-J). The FtsA filaments were again sandwiched between the liposome membrane and the FtsZ filaments, just as in the images obtained with *E. coli* cells (Figure 2C & G). The architecture is easily explained with TmFtsA binding to the inside of the liposome membrane via its amphipathic helix, presumably polymerising, and FtsZ polymerising

on top of FtsA, binding to it via its C-terminal FtsA binding peptide (Pichoff and Lutkenhaus, 2005; Szwedziak et al., 2012). Nucleotide presence had some influence on the appearance of these constricted liposomes as GTP addition produced the most bilobed liposomes. Constriction itself, however, was largely nucleotide hydrolysis independent since not adding any nucleotide produced constrictions as well, and they appeared even tighter (Figure 3E). Therefore, despite not being strictly required for constriction, we believe the nucleotide only has an influence on the appearance thereof and this might be due to the fact that FtsZ forms much longer filaments with polymerisation-inducing GTP added and this would enable the filaments to span larger liposomes when the process starts. Given that TmFtsZ is a hyperthermophilic protein, significant hydrolysis of GTP to GDP is not expected.

**Detailed architecture of the liposome constrictions revealed in three dimensions by electron cryotomography.**

Next we employed electron cryotomography to image the liposomes in three dimensions (Figure 4, Figure 4—figure supplement 1, Movies M4-M10). Because the samples only contained lipid and two proteins, contrast was very high in the resulting tomograms (Movie M4 & M5), making it possible to represent the volume data without segmentation, as single-threshold surfaces or as volume renderings (Movie M6-M10, Figure 4—source data 1 PyMOL session file). None of the figures or movies we present has been segmented, manually or automatically. Figure 4A, top shows a constricted liposome in stereo, highlighting the three distinct filament architectures in detail: arcs, spiral domes at the 'poles' and the filamentous ring, pulling and constricting the membrane. Note that the liposome was only deformed where the ring was located (and where it unfortunately touched the carbon grid at the top right). More examples in Figure 4A, bottom and Figure 4—figure supplement 1 show the

same overall architecture, with the same mix of filament architectures (also Movies M6-M10). The TmFtsAZ rings were between 30 and 90 nm in diameter when we looked at several different liposomes and the filaments were on average 7.8 nm apart ( $n = 16$ ) laterally (Figure 4B and C) as compared to 6.8 nm seen in *E. coli* cells (within doublets). Because contrast was very high, the ring of filaments could be traced in most tomograms all around the inside of the liposome and this revealed that the filaments were not totally equidistant and often came into contact. This was also true for the *in vivo* situation in *C. crescentus* (Movie M1) where the distance between the filaments (gray arrow) changes around the ring. The rings were always closed, continuous without gaps, with some possibly consisting of one double filament forming a helix (Figure 4—figure supplement 1 and Movie M6) and others containing several shorter filaments in a helix-like arrangement (Figure 4A stereo view and Movie M10). When the filaments were investigated end-on, they appeared to always be arranged close to 90° with respect to the liposome membrane tangent (Figure 4C), which was also observed for the filaments in cells (Figures 2C & G). All of these features are best demonstrated in Movie M10, which provides an overview of the constriction and filament architectures and should be consulted to appreciate these findings properly.

### **A semi-atomic model of the FtsZ ring constricting a liposome.**

Map quality allowed us to fit the FtsZ crystal structure manually and roughly through a spline curve and arrive at a pseudo-atomic model for an FtsZ ring (Figure 5A), making it possible to judge distances and dimensions relative to the crystal structures. A more detailed view using sphere representation (Figure 5B) shows, again, that the filaments within a ring were not exactly equidistant (black arrows) but came into direct contact only at certain points. Fitting the FtsA crystal structure into the map as

345 well revealed two closely associated filaments, and showed that the outline fit of the  
346 tomographic density is extremely good, although exact orientations and locations of  
347 the subunits along the filament of the molecules can only be guessed in most places  
348 given the resolution limit. It should be noted, though, that peaks appear in many  
349 places indicating the centre positions of individual FtsZ molecules (Figure 5C, Figure  
350 4—source data 1, a PyMOL session file).

351

**Discussion:****Constriction is accompanied by filament sliding.**

How do FtsZ and FtsA constrict liposomes? Is this likely to be related to the *in vivo* situation? Given that the filament architectures observed here in *C. crescentus* and *E. coli*, and in constricting liposomes are so similar we would suggest that the model we propose should be valid for both *in vitro* and *in vivo*, at least at some primordial level. FtsA forms (partial) filaments between the membrane and FtsZ filaments, and the filaments together encircle the constriction site while forming a single-layered small band of filaments. The entire structure is slightly helical and shorter filaments overlap to form a continuous, closed ring.

By imaging completely unmodified cells, utilising recent advances in cryo-EM and acquiring tomograms of cells parallel to the tilt axis we concluded that the FtsZ ring in cells is most likely continuous, probably made of shorter overlapping filaments. Previous analysis of *C. crescentus* cells by cryo-ET also showed that the FtsZ ring consists of overlapping filaments inside the inner membrane, although not all cells showed continuous rings (Li et al., 2007). Equally, results obtained with super resolution fluorescence microscopy techniques (Holden et al., 2014) showed punctuated fluorescence, possibly indicating non-continuous rings. We think it is important to point out that fluorescence microscopy only images the labelled species and intensity fluctuations within the ring may have arisen from using non-functional GFP fusions and/or their over-expression. Or fluctuations coming from overlapping filaments may have been over-emphasised during image analysis because of very low signal-to-noise. Unfortunately, currently, cellular tomography data is too weak to be able to trace individual filaments and their ends with confidence so we have no direct

evidence from our *in vivo* data for the length of individual FtsZ filaments making up continuous rings.

Given a continuous ring, at least in the *in vitro* situation, with no GTP turnover (or no added nucleotide) there is no filament shortening, meaning constriction requires the filaments to slide along each other as the ring decreases in diameter and the membrane deforms. That opposing forces from the filaments and the membrane surface are at work is most evident from the fact that the rings were always perfectly round, in contrast to the rest of the liposomes (Figure 4B, middle, Movie M10).

In this context the filament spirals that form shallow 'dome' structures in some of the liposomes and on flat monolayers (Figure 3A, 4A, top and Figure 4—figure supplement 1) are most revealing. They appear to be the result of sliding and condensation, and show decreasing filament curvature, but do not deform the lipid membrane. This can be explained because the constriction force, which acts in the plane of the spirals, will not exert any force on the membrane since it is tangential (Figure 5D, right). In contrast, if the filaments form a ring around the volume of the liposome (in the middle, not at the poles), the constriction force is perpendicular to the membrane and will lead to the membrane being pulled in (Figure 5D, left).

Since in this model force generation is dependent on a closed ring, the system becomes self-regulating since constriction will only commence after a complete ring has formed. If the cell is too large or not enough FtsZ is available, constriction will not begin. It is important to note that only a closed, continuous ring is required, but it may consist of a number of shorter, overlapping filaments (as it did in the liposome reconstitutions, Figure 4).

**Where is the energy coming from for sliding and constriction?**

What drives constriction of the closed rings and filament sliding? We propose three possible mechanisms that may even act in concert: (a) maximising filament overlap via sliding, (b) increasing repeat mismatch and (c) repeated filament shortening through nucleotide turnover.

(a) When the overlap between the filaments that are attracted to each other increases, more and more binding energy is produced. This has been proposed before to be theoretically sufficient for the constriction process (Lan et al., 2009) (Figure 5E). The lateral spacing of 6.5-8 nm between filaments we report here is slightly larger than the thickness of FtsZ filaments and presumably also FtsA filaments (Matsui et al., 2012; Szwedziak et al., 2012). Previous *in vitro* work reported an interfilament distance of 5 nm using FtsZ-mts, however, this was after negative staining and dehydration and no constrictions were observed, possibly due to lateral interactions being too tight (Milam et al., 2012). In *C. crescentus* cells the lateral spacing between filaments was found to be 9.3 nm previously (Li et al., 2007)(Li et al., 2007) and we report here distances of ~ 7.8 (Figure 1A) in *C. crescentus* and ~ 6.8 nm (Figure 1G) in *E. coli*. AFM using only FtsZ, but observing spiral condensation, provided an even larger distance of 12 nm (Mingorance et al., 2005). All of these measurements are averages with large variances. One may conclude that the filaments in the FtsZ ring interact transiently and direct contact is localised to only a few small regions within the ring at a time. This could facilitate the constriction process since the filaments have to be free to slide. It was suggested previously that instead of forming many intermolecular solid bonds, which would lead to avidity and a barrier to sliding, an attractive force over a longer distance would keep the filaments apart while interacting (Hörger et al., 2008). This is more akin to the liquid state of matter, where many transient homotypic

interactions, counteracted by thermal motion, lead to a fluid situation without absolute order but still keeping the molecules together.

(b) The second possible driver of constriction comes from the repeat length mismatch of FtsA and FtsZ (Szwedziak et al., 2012). Although it is evident from our data that the curvature of individual filaments can not deform liposomes significantly from the inside, the decreasing diameter of the ring accompanied by increasing membrane curvature might enable more and more FtsA to be added, until an optimum curvature of the system has been achieved (Figure 4—figure supplement 2); this could provide additional energy and would also explain why FtsA exists at all and FtsZ is not directly attached to the membrane.

(c) Why does FtsZ hydrolyse GTP then? We speculate that when constriction starts at large diameters (1  $\mu\text{m}$  in *E. coli*), longer GTP-induced FtsZ filaments are needed to reach reliably around the cell in order to produce overlap, for the ring and 'force engagement' to start the process. However, increasing overlap, developing as the constriction progresses, might lead to a kinetic barrier of sliding through avidity and the filaments would then have to be shortened. Formally this provides a third possible driver of constriction, at least for large constriction distances.

#### **Dynamics of the FtsZ ring are essential for its function.**

Continual depolymerisation and re-polymerisation through nucleotide turnover, as shown *in vivo* by FRAP (Stricker et al., 2002) might also ensure the ring never reaches a highly condensed state and FtsZ monomer-sequestering inhibitors such as Sula remain able to stop the process at any time (Chen et al., 2012). However, it has been reported that the GTP hydrolysis-deficient FtsZ(D212G) mutant generates prominent constrictions of tubular liposomes *in vitro* (Osawa and Erickson, 2011) and

functions in cell division in *E. coli* (Bi and Lutkenhaus, 1992; Osawa and Erickson, 2006; Trusca et al., 1998). Furthermore, the use of non-hydrolysable GTP analogues did not impair the formation of condensed FtsZ structures on mica (Hörger et al., 2008). Taken together with our result that constriction of liposomes may in principle be independent of GTP hydrolysis, these data question the alternative idea of force generation by filament bending upon GTP hydrolysis as has been suggested previously (Erickson et al., 2010; Li et al., 2013; Lu et al., 2000). We suggest that nucleotide binding/hydrolysis is required solely for filament growth/shrinkage as these are essential to maintain the dynamic state of the FtsZ ring in cells.

Taken together, we envisage that *in vitro* liposome constrictions and *in vivo* cell division quite possibly utilise a different set of energetic drivers (a-c); for example, GTP hydrolysis was not required *in vitro* but clearly plays a role *in vivo*. And of course, it is likely that cell wall synthesis in the periplasm, guided by the Z-ring through the divisome, provides additional force in cells. So far, wall-less bacterial L-forms have not shed light on this interdependence of cell wall synthesis and the FtsZ ring since artificial L-forms were found to divide by blebbing, most likely a mechanism that is not actively supported by cellular machinery (Leaver et al., 2009). FtsZ-based cell division is not functioning in these L-forms and we suggest this may be because L-forms are too large for Z-rings to close given the amounts of FtsAZ present.

#### **How to perform abscission?**

The described FtsZ filament arrangement might also provide a solution to the abscission problem: how do the membranes fuse at the end of division when the protein filaments are in between? Figure 5D, middle shows how an intermediate

between the rings and the domes (as is present in the liposome constriction shown in Figure 4A, bottom right and Movie M9) may explain abscission, since the protein ring would normally be in the way of membrane fusion/fission at the end. The change from a flat band of filaments towards the helical spirals enables inward force to be developed on each side of the constriction, with a helical spiral on each side. The spirals observed in the dome-like structures might even be remnants of such liposome abscission events, although we have no evidence for this (Figure 5D, right). It remains to be seen if FtsZ is involved in final abscission since it has recently been reported that FtsZ might leave the septum earlier (Söderström et al., 2014).

#### **Similarities to other membrane remodelling systems.**

It is important to mention that membrane constriction with ESCRT-III and dynamin filaments has also been suggested to involve sliding helical filaments (Guizetti et al., 2011; Roux et al., 2006) and similar arrangements to those depicted in Figure 5D, right were predicted for the ESCRT-III system (Fabrikant et al., 2009).

Finally, our reconstitution of cell division can easily be adapted to include other cell division proteins, such as the division site selection mechanism MinCDE, nucleoid occlusion, FtsZ cross-linkers such as ZapA and many more middle and outer divisome components.

## Experimental Procedures:

### *Plasmids and strains*

Plasmids used in this work are listed in Supplementary File 1A. *E. coli* DH5 $\alpha$  was used for cloning. *Caulobacter crescentus* NA1000/CB15N and *E. coli* B/r H266 (Trueba and Woldringh, 1980) were used for cellular electron cryotomography.

### *Cellular tomography sample preparation*

*Caulobacter crescentus* was grown overnight in PYE medium at 30°C. The overnight culture was used to inoculate 50 ml of M2G medium. The culture was grown at 30°C until the OD reached 0.5. 11  $\mu$ l of this culture were mixed with 1  $\mu$ l of protein-A conjugated to 10 nm gold beads (CMC, Leiden) and applied to freshly glow-discharged 300 mesh Cu/Rh Quantifoil (3.5/1) grids. The grids were plunge frozen into liquid ethane using a FEI Vitrobot (Mark IV) and stored in liquid nitrogen.

*E. coli* cells (some containing relevant plasmids, for FtsZ mutant co-expression with endogenous wild-type FtsZ, Supp. Table 1 & 2) were grown at 30°C in M9 minimal media supplemented with 0.4 % glycerol until log-phase. Cells were then diluted into fresh M9 media with 0.02 % arabinose (where needed, final concentration), and grown for 1-2 hours for FtsZ mutant protein expression.

### *Lipid monolayer assay*

*Thermotoga maritima* FtsZ (TmFtsZ) and FtsA (TmFtsA) proteins were purified and 2D monolayers were prepared as described previously (Szwedziak et al., 2012), taking extra care and verifying by ESMS that the C-terminal tails of both protein were intact after purification as they are prone to proteolytic cleavage as this was not obvious from gels, sometimes.

**514 *In vitro reconstitution of TmFtsZ and TmFtsA outside liposomes***

515 20 µl of *E. coli* total lipid extract (Avanti Polar Lipids, US) chloroform solution at 10  
516 mg/ml was dried in a glass vial (Wheaton, New Jersey, US) under a stream of  
517 nitrogen gas and left overnight under vacuum to remove traces of the solvent. The  
518 resulting thin lipid film was hydrated with 200 µl of TEN<sub>100</sub>7.5 buffer (50 mM  
519 Tris/HCl, 100 mM NaCl, 1 mM EDTA, 1 mM NaN<sub>3</sub>, pH 7.5) containing either  
520 TmFtsA at 20 µM or TmFtsZ at 60 µM or both proteins. After 10 minutes of  
521 incubation at room temperature the solutions were sonicated for 1 minute in a water  
522 bath sonicator and then 2.5 µl of sample was plunge-frozen onto Quantifoil R2/2  
523 holey carbon grids (Quantifoil, Germany) using an FEI Vitrobot (FEI, USA). Samples  
524 were stored in liquid nitrogen.

**525 *In vitro reconstitution of TmFtsZ and TmFtsA inside liposomes***

526 50 µl of *E. coli* total lipid extract chloroform solution at 10 mg/ml was dried in a glass  
527 vial under a stream of nitrogen gas and left overnight under vacuum to remove traces  
528 of the solvent. The resulting thin lipid film was hydrated with 50 µl of TEN<sub>100</sub>7.5 plus  
529 20 mM CHAPS (Anatrace), and shaken vigorously at 800 rpm using a benchtop  
530 Eppendorf shaker for 2 hours. The lipid-detergent solution was sonicated for 1 minute  
531 in a water bath sonicator. Subsequently, 50 µl of TmFtsZ (30 µM) and TmFtsA (10  
532 µM) solutions supplemented with 0.5 mM MgGTP or MgGMPCPP (Jena Bioscience,  
533 Germany) or no nucleotide was added and left for 30 minutes at room temperature.  
534 Next, the mixture was gradually diluted within 10 to 20 minutes to 600 µl with  
535 TEN<sub>100</sub>7.5 or TEN<sub>100</sub>7.5 plus nucleotides (both without detergent) to trigger  
536 spontaneous liposome formation. 2.5 µl of the solution was mixed with 0.2 µl 5 nm

537 IgG immunogold conjugate (TAAB, UK) and plunge-frozen onto Quantifoil R2/2  
538 holey carbon grid using an FEI Vitrobot.

539 ***Electron cryomicroscopy and cryotomography***

540 2D electron cryomicroscopy (cryo-TEM) images were taken on an FEI TECNAI  
541 Spirit TEM operating at 120 kV with a 2k x 2k CCD camera at a magnification of 42  
542 k, corresponding to a pixel size of 0.25 nm. For electron cryotomography, samples  
543 were imaged using an FEI Polara or FEI Titan Krios TEM operating at 300 kV,  
544 equipped with a Gatan imaging filter set at zero-loss peak with a slit-width of 20 eV.  
545 A Gatan Ultrascan 4000 CCD camera binned to 2k x 2k or a 4k x 4k K2 Summit  
546 direct electron detector was used for data acquisition with SerialEM software  
547 (Mastronarde, 2005). Cells or *in vitro* reconstituted systems were imaged at a  
548 magnification of 41 k, corresponding to a pixel size of 5.8 Å (with US4000), or at a  
549 magnification of 26 k, corresponding to a pixel size of 4.5 Å (for K2) at the specimen  
550 level. Specimens were tilted from approximately -60° to +60° ( $\pm 65^\circ$  for *C. crescentus*  
551 cells) with a 1° increment. The defocus was set to between 8 and 10  $\mu\text{m}$ , and the total  
552 dose for each tilt series was around 120  $\text{e}/\text{\AA}^2$  for *in vitro* reconstitution samples and  
553 150 - 200  $\text{e}/\text{\AA}^2$  for cells.

554 ***Image processing***

555 Tomographic reconstructions from tilt series were calculated using RAPTOR (Amat  
556 et al., 2008) and the IMOD tomography reconstruction package followed by SIRT  
557 reconstruction with the PRIISM software or the TOMO3D package (Agulleiro and  
558 Fernandez, 2011; Chen et al., 1996; Kremer et al., 1996). Measurements of distances  
559 between structures were carried out within IMOD. Movies showing liposomes were  
560 prepared with PyMOL (DeLano, 2002).

561 ***Structured illumination microscopy (SIM)***

562 *E. coli* B/r H266 cells with plasmid pMZ124 were grown in LB medium at 30 °C. At  
563 an OD<sub>600</sub> of 0.2, FtsZ(D212A) and FtsA expression was induced by adding 0.02 %  
564 arabinose. After 2 hours cell membranes were stained with FM4-64 membrane dye,  
565 and cells were mounted on an agarose pad and visualised using a Nikon N-SIM  
566 microscope in the 2D-SIM mode.

567 ***Western blot***

568 FtsZ expression level in cells used for electron cryotomography experiments were  
569 examined with Western blots using rabbit anti-FtsZ primary antibodies (Agrisera,  
570 Sweden) and donkey anti-rabbit IgG conjugated with horseradish peroxidase (GE  
571 Healthcare) and detected with ECL blotting reagent.

572 ***Database deposition***

573 The *Caulobacter crescentus* tomogram shown in Figure 1A has been deposited in the  
574 EM databank with accession number EMD-2814. The edited tomogram of TmFtsAZ  
575 constricting a liposome, as shown in Figure 4A, 5A and Movie M10 has been  
576 deposited with accession number EMD-2815.

**577 Acknowledgements:**

578 We are very grateful to Leonid Sazanov (MRC Mitochondrial Biology Unit,  
579 Cambridge UK) for the suggestion to use CHAPS-solubilised lipids for liposome  
580 formation. We would like to thank Colin Palmer, Shaoxia Chen and Christos Savva  
581 (MRC-LMB) for help with electron microscopy. Work on LMB's FEI Krios  
582 microscope was aided by Matthijn Vos and Sonja Welsch (FEI). Tom Goddard  
583 (UCSF) provided excellent help with spline fitting of the filaments. We would like to  
584 acknowledge access to a Nikon N-SIM microscope at the MRC Mitochondrial  
585 Biology Unit, Cambridge UK. This work was supported by the Medical Research  
586 Council (U105184326) and the Wellcome Trust (095514/Z/11/Z to JL).

587

588

589

590

591

592

593

594

595

596

597

598

599 **Figure Legends:**

600 **Figure 1. FtsZ forms bands of filaments completely encircling *C. crescentus* and**  
601 ***E. coli* division sites, as visualised by electron cryotomography.**

602 **(A)** *C. crescentus* NA1000/CB15N division site with filaments near the inner  
603 membrane IM (top panel, black dots highlighted by arrow, see also Movie M1).  
604 Bottom panel shows the same cell rotated 90° around the short axis of the cell. The Z  
605 ring (arrow) is continuous and only invisible where there is no image because of the  
606 missing wedge (shaded triangle) (see Figure 1—figure supplement 1 for more details  
607 on the missing wedge problem). The cytoplasm (beige), periplasm (blue) and space  
608 between the OM and S layer (cyan) have been coloured for clarity.

609 **(B)** More examples of continuous FtsZ rings found in *C. crescentus* cells. The  
610 filaments were on average 15 nm from the inner membrane.

611 **(C)** Electron cryotomographic slice of the constriction site of a B/r H266 *E. coli* cell  
612 visualised perpendicular to the longitudinal axis, showing very similar FtsZ filaments  
613 when compared to *C. crescentus* (Figure 1A & B) and FtsZ(D212A) expressing *E.*  
614 *coli* cells (Figure 1F) and having roughly the same distance (16 nm) to the IM. Movie  
615 M2 demonstrates the likely helical nature of the arrangement of the FtsZ filaments  
616 (see also Figure 1—figure supplement 2).

617 **(D)** Western blot showing total FtsZ levels in cells used in (E - G) are about 2.5 x  
618 that of wild-type cells. (+) refers to un-induced, (++) was induced by 0.02%  
619 arabinose. EcZ is purified *E. coli* FtsZ protein.

620 **(E-G)** 10 nm thick electron cryotomographic slices of *E. coli* cells expressing  
621 FtsZ(D212A) protein in a wild-type B/r H266 background. (See also Figure 1—figure  
622 supplement 3)

623 **(E)** *E. coli* division site showing the cross-section of FtsZ filaments (single row of  
624 black dots) at the constriction site. See Movie M3.

625 **(F)** Visualisation of the same along the longitudinal axis shows FtsZ filaments are  
626 located ~16 nm from the inner membrane (IM).

627 **(G)** Closer examination of the constriction site of another cell with higher expression  
628 level reveals FtsZ filaments form pairs, appearing as doublets of dark dots (upper) and  
629 orange spheres in the schematic illustration, on average 6.8 nm apart within the  
630 doublets (lower).

631 **(H-K)** 10 nm thick electron cryotomographic slices of *E. coli* cells expressing  
632 engineered protein constructs based on FtsZ(D212A) (see also Figure 1—figure  
633 supplements 3 & 5 and Table S2).

634 **(H)** Extending the C-terminal linker of FtsZ by inserting a linker sequence pushes the  
635 filaments further away from the IM (distance changed from 16 nm to a somewhat  
636 variable 16-21 nm).

637 **(I)** Replacing the C-terminal FtsA-binding sequence of FtsZ with a membrane-  
638 targeting sequence (mts) makes FtsZ directly bind to the IM and results in FtsZ  
639 filaments closer to IM (distance changed from 16 nm to 10 nm). No cell constrictions  
640 were observed with this construct.

641 **(J)** Removing the C-terminal FtsA-binding sequence of FtsZ renders it unable to  
642 maintain a fixed distance to the IM and FtsZ filaments were observed within the  
643 cytoplasm.

644 **(K)** Removing the C-terminal flexible linker of FtsZ makes it prone to form multiple  
645 layers of filaments that form complete rings or helices. Tomography using this  
646 construct works better because it produces small minicells.

(L) A closer inspection of the area marked with the black arrowhead in G shows beads along the filament as illustrated by the schematic drawing with a repeat distance of 4 nm as expected for FtsZ filaments.

*IM: inner membrane; OM: outer membrane; WT: wild-type; Q-rich: FtsN-derived flexible linker; mts: membrane-targeting sequence. Scale bars: 100 nm in (A) and (B), 50 nm in (E, F, H, I, J), 20 nm in (C, G, K), 10 nm in (H), 20 nm in (L).*

**Figure 2. Co-expression of FtsZ and FtsA in *E. coli* cells leads to extra septa.**

(A) A low-magnification 2D electron cryomicrograph (transmission) showing multiple constriction sites (marked with black arrowheads) along the cell.

(B-E) 10 nm thick electron cryotomographic slices of cells co-expressing FtsZ(D212A) and FtsA (bicistronic, 1:1). Two layers of dots are visible at constriction sites in (B) and (C), corresponding to FtsZ filaments and FtsA filaments, respectively, as labelled in the orthogonal view along the long axis of the cell (D). FtsA filaments are almost in the middle between FtsZ filaments and the IM, at a distance of 8 nm from both FtsZ filament and IM as indicated in (E).

(F) Structured illumination microscopy images of cells expressing FtsZ(D212A) and FtsA, showing cell division and minicell formation, proving that the extra septa function to completion.

(G) 10 nm thick electron cryotomographic slice of an *E. coli* minicell formed from cells expressing *Thermotoga maritima* FtsZ and FtsA proteins, with a deeply constricted area showing cross-sections of FtsZ and FtsA filaments (black dots marked with white arrows). Distance between FtsZ filaments and IM is around 12 nm

(inset in G). The view highlights striking similarities to the *in vitro* reconstruction shown in Figures 3H-J & 5C.

*IM: inner membrane; OM: outer membrane. Scale bars: 500 nm in (A), 100 nm in (B), 10 nm in (C, and also for inset in G), 20 nm in (E, and also for D), 2  $\mu$ m in (F).*

**Figure 3. *In vitro* reconstitution of bacterial cell membrane constriction by the FtsZ ring from purified components.**

**(A)** *Thermotoga maritima* FtsA (TmFtsA) and *Thermotoga maritima* FtsZ (TmFtsZ) form spirals on a flat lipid monolayer, as indicated by a white dotted line. The filaments tend to appear as double strands (doublets). Negative-stain electron microscopy.

**(B)** Transmission electron cryomicroscopy allows resolution of the inner and outer leaflet of undisturbed liposomes (top panel). When TmFtsA is added to the outside, an additional layer of density corresponding to FtsA becomes apparent (middle panel). Recruitment of TmFtsZ by TmFtsA leads to the formation of two layers (bottom panel). Taken together, we conclude that FtsA is sandwiched between the membrane and FtsZ filaments (bottom panel). (See also Figure 3—figure supplement 1 and Figure 3—figure supplement 2)

**(C-G)** Constriction sites are efficiently formed when TmFtsA and TmFtsZ are encapsulated in liposomes that have sizes comparable to bacterial cells. Five representative liposomes are shown using transmission electron cryomicroscopy (hence are 2D projections of 3D objects). Importantly, constriction sites are only formed where a ring made of the two proteins is present (black arrowheads) and not at other sites where filaments are located. The TmFtsA and TmFtsZ layers are clearly

visible (inset H, same as boxed area '1' in C; inset J, same as boxed area '2' in C and inset I, which is from Figure 4 electron cryotomography data) and the protein's organisation mirrors that present in *E. coli* cells (compare with Fig. 2C). The distance of 12 nm between TmFtsZ and the membrane (inset J) resembles that found in overexpressing cells (see Fig. 2G and also 5C). (E) Intriguingly, liposomes are being constricted (partially) in the absence of added nucleotide.

*Scale bars: 50 nm in (A-C), 25 nm for insets*

**Figure 4. Electron cryotomography of liposomes constricted *in vitro* by rings of TmFtsA and TmFtsZ.**

(A) Stereo view of a representative liposome highlighting three different structures made by the enclosed TmFtsA and TmFtsZ proteins. Note that our images derived from tomographic volume data have not been segmented, they are volume representations of the actual 3D tomographic data. Arcs (also on the outside) are filaments made of both FtsA and FtsZ, whose curvature is determined by the mismatch in TmFtsA and TmFtsZ polymers subunit spacing (5 vs. 4 nm, see also Figure 3—figure supplement 1 & Figure 4—figure supplement 2). Dome-like structures are slightly helical spirals of condensing TmFtsZ filaments attached to the membrane by TmFtsA. Importantly, only complete rings seem capable of constriction force generation. The ring might consist of overlapping filaments (as in the stereo view and Movie M10) or maybe a continuous helix of double filaments (bottom panel, middle liposome with black arrowheads, see also Figure 4—figure supplement 1 and Movie M6). The bottom panel depicts more examples of different liposome shapes and sizes. The cross-section (right) shows the distribution of filaments (red)

inside a liposome (membrane in blue) (bottom right). Movie M4 shows a complete 3D volume in grey scale. Movie M5 shows a slice view at high magnification, demonstrating the excellent contrast these specimen generate, making it possible to see individual subunits and complete filament traces. Movies M6 to M9 show 3D views of several constricted liposomes. Figure 4—source data 1 enables 3D viewing of a liposome volume with PyMOL.

**(B)** Close-up view of the FtsZ ring (purple) attached to the membrane (blue), here shown as single-threshold surface representations (these are not automatic or manual segmentations). The filaments overlap and interact laterally (left panel). View along the long axis shows that the ring is a perfect, closed circle (middle panel). The black arrow points to where TmFtsZ and TmFtsA filaments are fully detached from each other. Individual filaments are resolved (right panel). Movie M10 shows a 3D walk-through the liposome, highlighting most features on the way.

**(C)** Comparison of filament arrangements and geometries within the dome-like structures (left panel) and ring-like structures (right panel). Cross-sections demonstrate that in both cases the TmFtsAZ filaments are positioned at close to perpendicular with respect to the membrane (red symbols). However, the constriction force is generated only in the rings (see Figure 5D for explanation).

### **Figure 5. Visualising the FtsZ ring at the molecular level.**

**(A)** A semi-atomic model of the FtsZ ring constricting a liposome. 294 monomers of *S. aureus* FtsZ have been roughly positioned using a spline-fitting approach (PDB 3VO8 (Matsui et al., 2012)). This uses the same tomography data as Figure 4A.

**(B)** The ring is 90 nm in diameter (left) and 60 nm thick (middle). It consists of at least four individual filaments (right, atoms shown as spheres) with varying lateral interfilament distances (right, atoms shown as spheres, black arrows).

**(C)** FtsZ filaments are single protofilaments but they tend to pair in doublets. A precision manual fit of the TmFtsA polymer crystal structure (PDB 4A2B) (Szwedziak et al., 2012) in addition to 3VO8 FtsZ polymer crystal structure was performed in a region of very good density. The fit is excellent and dimensions and distances match well CcFtsZ, EcFtsZ and TmFtsAZ *in vivo* situations (Figures 1A, 1E, 2E & 2G).

**(D)** Left: in the ring-like structures (black), force (red arrows) is perpendicular to the membrane (blue), leading to constriction. Middle: during constriction, the ring develops into two helical spirals, leading to forces pushing membrane inwards, and this might explain how abscission is accomplished since membranes will presumably not fuse while the protein filaments are in between (see Figure 4A bottom right and Movie M9 for an example of this in liposomes). Right: the domes we observed do not deform liposomes because the force generated is almost perfectly tangential to the membrane.

**(E)** Constriction force generation and filament sliding. In the discussion, three different energy sources for constriction are listed: maximising filament overlap, repeat-mismatch within FtsA-FtsZ copolymers (Figure 4—figure supplement 2) and filament shortening and turnover due to nucleotide hydrolysis by FtsAZ. While it is currently not obvious which of these, or if a combination of the three mechanisms drives constriction, it seems clear to us that constriction, at least in the liposome reconstitution experiments, requires filaments to slide past each other as is depicted in

two dimensions. Since also unmodified wild type cells (Figure 1) show closed, continuous rings at division sites, we would assume the same holds true *in vivo*. Filament sliding can also explain the spirals on lipid monolayers (Figure 3A) and spirals in the dome-like structures with liposomes (Figure 4A). The schematic drawn is a simplification into two dimensions, of course, *in vivo* and *in vitro* FtsZ filaments overlap in the third dimension, forming single-layered bands since each filament is anchored to the membrane.

**Legends figure supplements, source data file, supplementary file and movies:**

**Figure 1—figure supplement 1. The missing wedge problem in cellular electron cryotomography.** Since it is impossible to tilt the sample support (EM grids) from  $-90^\circ$  to  $+90^\circ$  and because the thickness of the ice film increases at high tilt angles, electron tomograms miss significant amounts of data. **(A)** Simulation of the effects of the missing wedge. Modified from (Palmer and Löwe, 2013). A phantom image resembling a cell envelope was reconstructed for a full  $\pm 90^\circ$  range and a  $\pm 60^\circ$  range, the latter being typical for tilt series acquisition. **(B)** Schematic drawings explaining the angle (blue) between the tilt axis (red) and the cell axis (black dashed line) and the missing wedge angle (green). The former can be anything between  $0$  and  $90^\circ$  whereas the latter anything between  $0$  and  $180^\circ$ . Tilt series for the *C. crescentus* study (Figure 1A-B) were obtained using the  $\pm 65^\circ$  range. **(C)** Examples of the effects of different orientations of cells in the microscope with respect to the tilt axis on the missing wedge. Cells that were aligned with the tilt axis produced the most complete tomograms since the cell thickness stayed constant over the angular range. High tilts of those perpendicular to the tilt axis did not provide any useful information since the effective cell thickness in the electron beam increased. Shown are projections along the long axis of the cell. It is important to note that whereas the angle between the tilt axis and the longitudinal axis of the cell is crucial in order to obtain high quality tilt series, other factors such as cell thickness, ice thickness and membrane invagination progression affect the quality of the resulting tomograms significantly. Scale bar: 100 nm.

**Figure 1—figure supplement 2. Electron cryotomograms of wild-type *E. coli* cells show filaments at the constriction sites.** (A, C) 10 nm thick tomographic slices of two cells showing black dots near the constriction sites corresponding to cross-sections of filaments. Filaments are difficult to discern in this viewing direction because of the thick *E. coli* cells (B, D) Filaments are better visualised when viewed perpendicular to the constriction planes showing filaments near the IM. These images, together with Movie M2, suggest that FtsZ forms a closed ring with slight helicity near the constriction site.

**Figure 1—figure supplement 3. FtsZ forms bands of filaments at constriction sites in *E. coli* cells.** (A) 10 nm electron cryotomographic slice of a cell expressing more FtsZ(D212A) protein than in Figure 1E (corresponds to Figure 1G), oriented parallel to the longitudinal axis, showing one layer of dots near the constriction site, corresponding to cross-sections of FtsZ filaments that are 16 nm away from the IM. (B) Electron cryotomographic slice of the cell viewed perpendicular to the dashed line in (A). FtsZ filaments and their relative position to the IM are illustrated with the schematic representation of the tomographic slice in (C); (D-E) 10 nm electron cryotomographic slices of a cell with very low level expression of FtsZ(D212A) protein (un-induced) viewed parallel to the longitudinal axis in (D) and perpendicular to the dashed line in (E), showing similar architecture of FtsZ filaments at the constriction site. Scale bars: 100 nm.

**Figure 1—figure supplement 4. Engineered FtsZ proteins form filaments with altered localisation patterns in *E. coli* cells.** (A) Extending the C-terminal flexible linker of FtsZ(D212A) makes the protein form filaments further away from the membrane with a distance to IM increased from 16 nm to 21 nm; (B) and (C) are tomographic slices of the cell viewed perpendicular to the dashed lines in (A) and

segmentation illustrating the relative positions of FtsZ filaments and the IM; **(D)** Cells expressing a membrane-binding FtsZ construct produced by fusing the *E. coli* MinD membrane-targeting sequence (mts) to the C-terminus of FtsZ produce filaments that are 10 nm away from IM; **(E)** Removing the C-terminal FtsA-binding sequence of FtsZ gives filaments further away from the IM; **(F)** FtsZ without the C-terminal flexible linker tends to form multiple layers of filaments near the constriction site, and such filaments appear to form complete rings or helices when viewed perpendicular to the plane of cell constriction. Scale bars: 100 nm.

**Figure 1—figure supplement 5. Overview of FtsZ constructs used for *in vivo* tomography.** Please also consult Supplementary File 1A & 1B.

**Figure 3—figure supplement 1. TmFtsZ and TmFtsA on the outside of liposomes and in the presence of GMPCPP deform liposomes.** **(A)** Low magnification (upper panel). More detailed snapshots (lower panel) show that the filaments are on the outside, however, they do not form rings but curved structures that are positioned in areas of negative membrane curvature that they probably induce. **(B)** Schematic representation of the curvature produced by co-polymerisation of FtsA and FtsZ, which have differing repeat distances of 5 and 4 nm, respectively. Since FtsA binds to the membrane, this arrangement will lead to negative curvature. Hence, the intrinsic, negative curvature of the FtsA:FtsZ filaments fits the curvature of the membrane on the inside. However, on the outside the membrane curvature is positive, as is also shown in Figure S8.

**Figure 3—figure supplement 2. Control experiments showing that both TmFtsA and TmFtsZ form straight filaments when polymerised separately. And liposomes deform mostly after dilution.** **(A)** When mixed, FtsA and FtsZ form

curved filaments (right panel). **(B)** TmFtsZ does not bind to liposomes on its own. Random electron cryomicroscopy images taken immediately after detergent dilution were analysed for liposome deformations. The plot in **(C)** shows the number of liposomes, out of 63, that are perfectly round (as per solidity quantity, defined in ImageJ). Clearly, liposomes become more deformed over a 30 min period after dilution. **(D)** Shows a spherical liposome without proteins added and **(E)** at time point 0 minutes, right after dilution. Scale bars 50 nm.

**Figure 4—figure supplement 1. Constrictions occur only at the site of filament ring formation.** A stereo view of the liposome marked with the black arrowheads in Figure 4A (bottom middle panel). A single helix made of filament doublets is marked with red arrow. Movie M6 shows its architecture in more details and in 3D.

**Figure 4—figure supplement 2. A mechanism explaining variable intrinsic FtsA:FtsZ filament curvature.** At some stages of constriction the ratio of FtsZ to FtsA in the ring may be higher than one. Normally, there is around five times more FtsZ in cells than FtsA), therefore only a few FtsA molecules may be sandwiched in between the IM and FtsZ filaments (which form more easily than FtsA filaments), upper panel. As curvature increases, the mismatch of the FtsA (orange) and FtsZ (grey) repeats (5 vs. 4 nm, respectively) makes it possible to add more FtsA since the double filament 'wants' to bend. Full occupancy of both FtsA and FtsZ in the double filament leads to a curvature of about 60 nm. This mechanism could be another source of energy for constriction in addition to or alternative to the condensation energy gained from filament overlap (mechanism b) in the discussion).

**Figure 4—source data 1.** PyMOL (version 1.7) session file showing volume and surface renderings of the liposome in stereo in Figure 4A, top. Note that this version

of the data has been volume edited, removing some of the filaments in the surroundings of the liposome. Nothing has been changed on the surface. These representations have not been segmented (automatically or manually); they show the volume data points as present in the (edited) tomogram. Both surface (threshold) as well as volume data are available as objects ‘surf’ and ‘vol’, respectively.

**Supplementary File 1.** (A) Plasmids used in this study. (B) Exact protein sequences of modified *E. coli* FtsZ proteins used for in vivo tomography experiments.

**Movie M1. Tomogram of a wild-type *C. crescentus* cell showing tomographic slices parallel to the longitudinal axis of the cell.** A single layer of dark dots corresponding to cross-sections of FtsZ filaments is clearly visible at a distance from the membrane on both sides of the septum. The missing wedge is located top and bottom. The distance between adjacent filaments highlighted by the arrow varies along the z-direction. Corresponds to Figure 1A.

**Movie M2. Tomogram of a wild-type *E. coli* cell showing the constriction site along the longitudinal axis of the cell.** FtsZ filaments are visible in certain slices, and are likely to be forming continuous helices indicated by its pattern when viewed along the slices. Corresponds to Figure 1C.

**Movie M3. Tomogram: FtsZ(D212A) expressed in *E. coli* cell forms doublet FtsZ filaments at the constriction site.** The movie shows tomographic slices parallel to the longitudinal axis of the cell. One single layer of dark dots corresponding to cross-sections of FtsZ filaments is clearly visible, and these dark dots tend to form pairs suggesting a doublet FtsZ filament architecture at the constriction sites formed with FtsZ and FtsZ(D212A). Corresponds to Figure 1E.

894 **Movie M4.** This movie shows a typical field of view from tomographic  
895 **reconstruction of the *in vitro* reconstitution specimen.** The filaments present on the  
896 water/air interface consist of TmFtsA and TmFtsZ filaments, and therefore adopt a  
897 curved geometry. Corresponds to Figure 4A.

898 **Movie M5.** This movie shows a volume of the liposome whose stereo view is  
899 depicted in Figure 4A.

900 **Movie M6.** This movie shows a volume representation of the liposome that is  
901 depicted in Figure 4A (bottom middle panel, black arrowheads) and whose stereo  
902 view is shown in Figure 4—figure supplement 1.

903 **Movie M7 and M8.** These movies show the two remaining liposomes that are  
904 depicted in Figure 4A.

905 **Movie M9.** This movie shows a well-pronounced constriction with spirals being very  
906 prominent on lateral sides of the leading membrane edge, which eventually might lead  
907 to abscission. Not shown in any other Figure. See also Figure 5D, middle for an  
908 explanation.

909 **Movie M10.** This movie runs through a surface representation of the liposome whose  
910 stereo view is depicted in Figure 4A, top, with features of interest highlighted along  
911 the way.

912 **References:**

- 913 Adams, D. W., and Errington, J. (2009). Bacterial cell division: assembly,  
914 maintenance and disassembly of the Z ring. *Nat Rev Microbiol* 7, 642-653.
- 915 Agulleiro, J. I., and Fernandez, J. J. (2011). Fast tomographic reconstruction on  
916 multicore computers. *Bioinformatics* 27, 582-583.
- 917 Amat, F., Moussavi, F., Comolli, L. R., Elidan, G., Downing, K. H., and Horowitz,  
918 M. (2008). Markov random field based automatic image alignment for electron  
919 tomography. *J Struct Biol* 161, 260-275.
- 920 Begg, K., Nikolaichik, Y., Crossland, N., and Donachie, W. D. (1998). Roles of FtsA  
921 and FtsZ in activation of division sites. *J. Bacteriol.* 180, 881-884.
- 922 Bernhardt, T. G., and de Boer, P. A. (2005). SlmA, a nucleoid-associated, FtsZ  
923 binding protein required for blocking septal ring assembly over Chromosomes in *E.*  
924 *coli*. *Mol Cell* 18, 555-564.
- 925 Bi, E., and Lutkenhaus, J. (1992). Isolation and characterization of ftsZ alleles that  
926 affect septal morphology. *J. Bacteriol.* 174, 5414-5423.
- 927 Bi, E. F., and Lutkenhaus, J. (1991). FtsZ ring structure associated with division in  
928 *Escherichia coli*. *Nature* 354, 161-164.
- 929 Buske, P. J., and Levin, P. A. (2013). A flexible C-terminal linker is required for  
930 proper FtsZ assembly in vitro and cytokinetic ring formation in vivo. *Mol. Microbiol.*  
931 89, 249-263.
- 932 Chen, H., DD, H., Chan, T. A., Sedat, J. W., and Agard, D. A. (1996). IVE (Image  
933 Visualization Environment): a software platform for all three-dimensional microscopy  
934 applications. *J Struct Biol* 116, 56-60.
- 935 Chen, Y., Milam, S. L., and Erickson, H. P. (2012). SulA inhibits assembly of FtsZ by  
936 a simple sequestration mechanism. *Biochemistry* 51, 3100-3109.

- 937 Dajkovic, A., Lan, G., Sun, S. X., Wirtz, D., and Lutkenhaus, J. (2008). MinC  
938 spatially controls bacterial cytokinesis by antagonizing the scaffolding function of  
939 FtsZ. *Curr Biol* 18, 235-244.
- 940 DeLano, W. L. (2002). The PyMOL Molecular Graphics System. DeLano Scientific  
941 San Carlos, CA, USA.
- 942 Erickson, H. P. (2009). Modeling the physics of FtsZ assembly and force generation.  
943 *Proc. Natl. Acad. Sci. U. S. A.* 106, 9238-9243.
- 944 Erickson, H. P., Anderson, D. E., and Osawa, M. (2010). FtsZ in bacterial  
945 cytokinesis: cytoskeleton and force generator all in one. *Microbiol Mol Biol Rev* 74,  
946 504-528.
- 947 Erickson, H. P., Taylor, D. W., Taylor, K. A., and Bramhill, D. (1996). Bacterial cell  
948 division protein FtsZ assembles into protofilament sheets and minirings, structural  
949 homologs of tubulin polymers. *Proc. Natl. Acad. Sci. U. S. A.* 93, 519-523.
- 950 Fabrikant, G., Lata, S., Riches, J. D., Briggs, J. A., Weissenhorn, W., and Kozlov, M.  
951 M. (2009). Computational model of membrane fission catalyzed by ESCRT-III. *PLoS*  
952 *Comput Biol* 5, doi: 10.1371/journal.pcbi.1000575.
- 953 Gardner, K. A., Moore, D. A., and Erickson, H. P. (2013). The C-terminal linker of  
954 *Escherichia coli* FtsZ functions as an intrinsically disordered peptide. *Mol. Microbiol.*  
955 89, 264-275.
- 956 Guizetti, J., Schermelleh, L., Mantler, J., Maar, S., Poser, I., Leonhardt, H., Muller-  
957 Reichert, T., and Gerlich, D. W. (2011). Cortical constriction during abscission  
958 involves helices of ESCRT-III-dependent filaments. *Science* 331, 1616-1620.
- 959 Holden, S. J., Pengo, T., Meibom, K. L., Fernandez Fernandez, C., Collier, J., and  
960 Manley, S. (2014). High throughput 3D super-resolution microscopy reveals  
961 *Caulobacter crescentus* in vivo Z-ring organization. *Proc. Natl. Acad. Sci. U. S. A.*
- 962 Hörger, I., Velasco, E., Mingorance, J., Rivas, G., Tarazona, P., and Velez, M. (2008).  
963 Langevin computer simulations of bacterial protein filaments and the force-generating

- 964 mechanism during cell division. *Phys Rev E Stat Nonlin Soft Matter Phys* 77,  
965 011902.
- 966 Hu, Z., and Lutkenhaus, J. (2003). A conserved sequence at the C-terminus of MinD  
967 is required for binding to the membrane and targeting MinC to the septum. *Mol.*  
968 *Microbiol.* 47, 345-355.
- 969 Kremer, J. R., Mastronarde, D. N., and McIntosh, J. R. (1996). Computer  
970 visualization of three-dimensional image data using IMOD. *J Struct Biol* 116, 71-76.
- 971 Lan, G., Daniels, B. R., Dobrowsky, T. M., Wirtz, D., and Sun, S. X. (2009).  
972 Condensation of FtsZ filaments can drive bacterial cell division. *Proc. Natl. Acad.*  
973 *Sci. U. S. A.* 106, 121-126.
- 974 Lara, B., Rico, A. I., Petruzzelli, S., Santona, A., Dumas, J., Biton, J., Vicente, M.,  
975 Mingorance, J., and Massidda, O. (2005). Cell division in cocci: localization and  
976 properties of the *Streptococcus pneumoniae* FtsA protein. *Mol. Microbiol.* 55, 699-  
977 711.
- 978 Leaver, M., Dominguez-Cuevas, P., Coxhead, J. M., Daniel, R. A., and Errington, J.  
979 (2009). Life without a wall or division machine in *Bacillus subtilis*. *Nature* 457, 849-  
980 853.
- 981 Li, Y., Hsin, J., Zhao, L., Cheng, Y., Shang, W., Huang, K. C., Wang, H. W., and Ye,  
982 S. (2013). FtsZ protofilaments use a hinge-opening mechanism for constrictive force  
983 generation. *Science* 341, 392-395.
- 984 Li, Z., Trimble, M. J., Brun, Y. V., and Jensen, G. J. (2007). The structure of FtsZ  
985 filaments in vivo suggests a force-generating role in cell division. *EMBO J.* 26, 4694-  
986 4708.
- 987 Loose, M., and Mitchison, T. J. (2014). The bacterial cell division proteins FtsA and  
988 FtsZ self-organize into dynamic cytoskeletal patterns. *Nat Cell Biol* 16, 38-46.
- 989 Löwe, J., and Amos, L. A. (1998). Crystal structure of the bacterial cell-division  
990 protein FtsZ. *Nature* 391, 203-206.

- 991 Lu, C., Reedy, M., and Erickson, H. P. (2000). Straight and curved conformations of  
992 FtsZ are regulated by GTP hydrolysis. *J. Bacteriol.* *182*, 164-170.
- 993 Lutkenhaus, J., Pichoff, S., and Du, S. (2012). Bacterial cytokinesis: From Z ring to  
994 divisome. *Cytoskeleton (Hoboken)* *69*, 778-790.
- 995 Ma, X., and Margolin, W. (1999). Genetic and functional analyses of the conserved  
996 C-terminal core domain of Escherichia coli FtsZ. *J. Bacteriol.* *181*, 7531-7544.
- 997 Margolin, W. (2012). The price of tags in protein localization studies. *J. Bacteriol.*  
998 *194*, 6369-6371.
- 999 Mastronarde, D. N. (2005). Automated electron microscope tomography using robust  
1000 prediction of specimen movements. *J Struct Biol* *152*, 36-51.
- 1001 Matsui, T., Yamane, J., Mogi, N., Yamaguchi, H., Takemoto, H., Yao, M., and  
1002 Tanaka, I. (2012). Structural reorganization of the bacterial cell-division protein FtsZ  
1003 from Staphylococcus aureus. *Acta Crystallogr D Biol Crystallogr* *68*, 1175-1188.
- 1004 Milam, S. L., Osawa, M., and Erickson, H. P. (2012). Negative-stain electron  
1005 microscopy of inside-out FtsZ rings reconstituted on artificial membrane tubules  
1006 show ribbons of protofilaments. *Biophys. J.* *103*, 59-68.
- 1007 Mingorance, J., Tadros, M., Vicente, M., Gonzalez, J. M., Rivas, G., and Velez, M.  
1008 (2005). Visualization of single Escherichia coli FtsZ filament dynamics with atomic  
1009 force microscopy. *J. Biol. Chem.* *280*, 20909-20914.
- 1010 Mukherjee, A., and Lutkenhaus, J. (1994). Guanine nucleotide-dependent assembly of  
1011 FtsZ into filaments. *J. Bacteriol.* *176*, 2754-2758.
- 1012 Oliva, M. A., Cordell, S. C., and Löwe, J. (2004). Structural insights into FtsZ  
1013 protofilament formation. *Nat Struct Mol Biol* *11*, 1243-1250.
- 1014 Osawa, M., Anderson, D. E., and Erickson, H. P. (2008). Reconstitution of contractile  
1015 FtsZ rings in liposomes. *Science* *320*, 792-794.
- 1016 Osawa, M., Anderson, D. E., and Erickson, H. P. (2009). Curved FtsZ protofilaments  
1017 generate bending forces on liposome membranes. *EMBO J.* *28*, 3476-3484.

- 1018 Osawa, M., and Erickson, H. P. (2006). FtsZ from divergent foreign bacteria can  
1019 function for cell division in *Escherichia coli*. *J. Bacteriol.* *188*, 7132-7140.
- 1020 Osawa, M., and Erickson, H. P. (2011). Inside-out Z rings--constriction with and  
1021 without GTP hydrolysis. *Mol. Microbiol.* *81*, 571-579.
- 1022 Osawa, M., and Erickson, H. P. (2013). Liposome division by a simple bacterial  
1023 division machinery. *Proc. Natl. Acad. Sci. U. S. A.* *110*, 11000-11004.
- 1024 Palmer, C. M., and Löwe, J. (2013). A cylindrical specimen holder for electron cryo-  
1025 tomography. *Ultramicroscopy* *137*, 20-29.
- 1026 Pichoff, S., and Lutkenhaus, J. (2005). Tethering the Z ring to the membrane through  
1027 a conserved membrane targeting sequence in FtsA. *Mol. Microbiol.* *55*, 1722-1734.
- 1028 Pichoff, S., and Lutkenhaus, J. (2007). Identification of a region of FtsA required for  
1029 interaction with FtsZ. *Mol. Microbiol.* *64*, 1129-1138.
- 1030 Redick, S. D., Stricker, J., Briscoe, G., and Erickson, H. P. (2005). Mutants of FtsZ  
1031 targeting the protofilament interface: effects on cell division and GTPase activity. *J.*  
1032 *Bacteriol.* *187*, 2727-2736.
- 1033 Rico, A. I., Krupka, M., and Vicente, M. (2013). In the beginning, *Escherichia coli*  
1034 assembled the proto-ring: an initial phase of division. *J. Biol. Chem.* *288*, 20830-  
1035 20836.
- 1036 Roux, A., Uyhazi, K., Frost, A., and De Camilli, P. (2006). GTP-dependent twisting  
1037 of dynamin implicates constriction and tension in membrane fission. *Nature* *441*, 528-  
1038 531.
- 1039 Rueda, S., Vicente, M., and Mingorance, J. (2003). Concentration and assembly of the  
1040 division ring proteins FtsZ, FtsA, and ZipA during the *Escherichia coli* cell cycle. *J.*  
1041 *Bacteriol.* *185*, 3344-3351.
- 1042 Söderström, B., Skoog, K., Blom, H., Weiss, D. S., von Heijne, G., and Daley, D. O.  
1043 (2014). Disassembly of the divisome in *Escherichia coli*: evidence that FtsZ  
1044 dissociates before compartmentalization. *Mol. Microbiol.* *92*, 1-9.

- 1045 Stricker, J., Maddox, P., Salmon, E. D., and Erickson, H. P. (2002). Rapid assembly  
1046 dynamics of the *Escherichia coli* FtsZ-ring demonstrated by fluorescence recovery  
1047 after photobleaching. *Proc. Natl. Acad. Sci. U. S. A.* 99, 3171-3175.
- 1048 Szwedziak, P., Wang, Q., Freund, S. M., and Löwe, J. (2012). FtsA forms actin-like  
1049 protofilaments. *EMBO J.* 31, 2249-2260.
- 1050 Trueba, F. J., and Woldringh, C. L. (1980). Changes in cell diameter during the  
1051 division cycle of *Escherichia coli*. *J. Bacteriol.* 142, 869-878.
- 1052 Trusca, D., Scott, S., Thompson, C., and Bramhill, D. (1998). Bacterial SOS  
1053 checkpoint protein Sula inhibits polymerization of purified FtsZ cell division protein.  
1054 *J. Bacteriol.* 180, 3946-3953.
- 1055 van den Ent, F., and Löwe, J. (2000). Crystal structure of the cell division protein  
1056 FtsA from *Thermotoga maritima*. *EMBO J.* 19, 5300-5307.
- 1057 Woldringh, C. L. (1976). Morphological analysis of nuclear separation and cell  
1058 division during the life cycle of *Escherichia coli*. *J. Bacteriol.* 125, 248-257.

Figure I

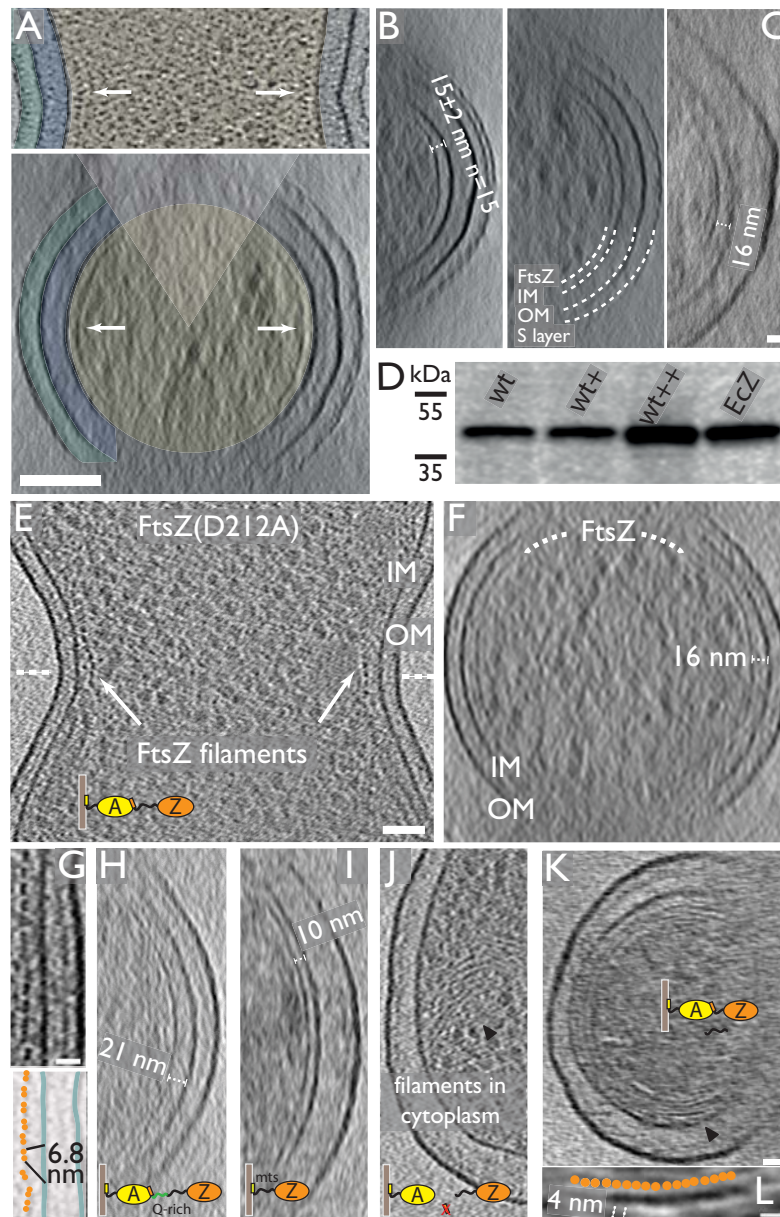


Figure 2

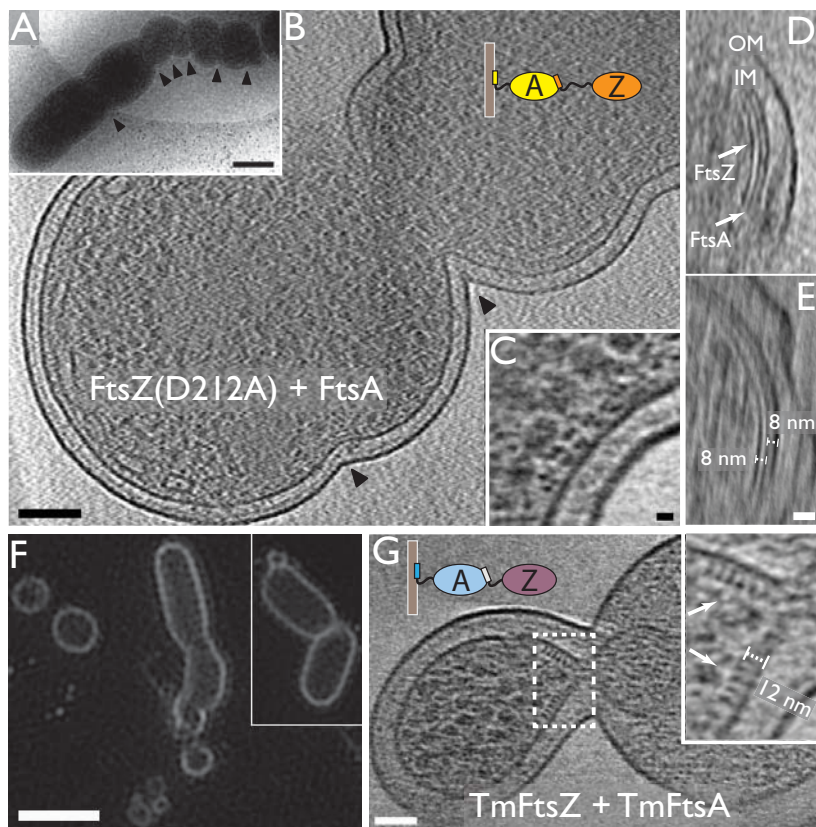


Figure 3

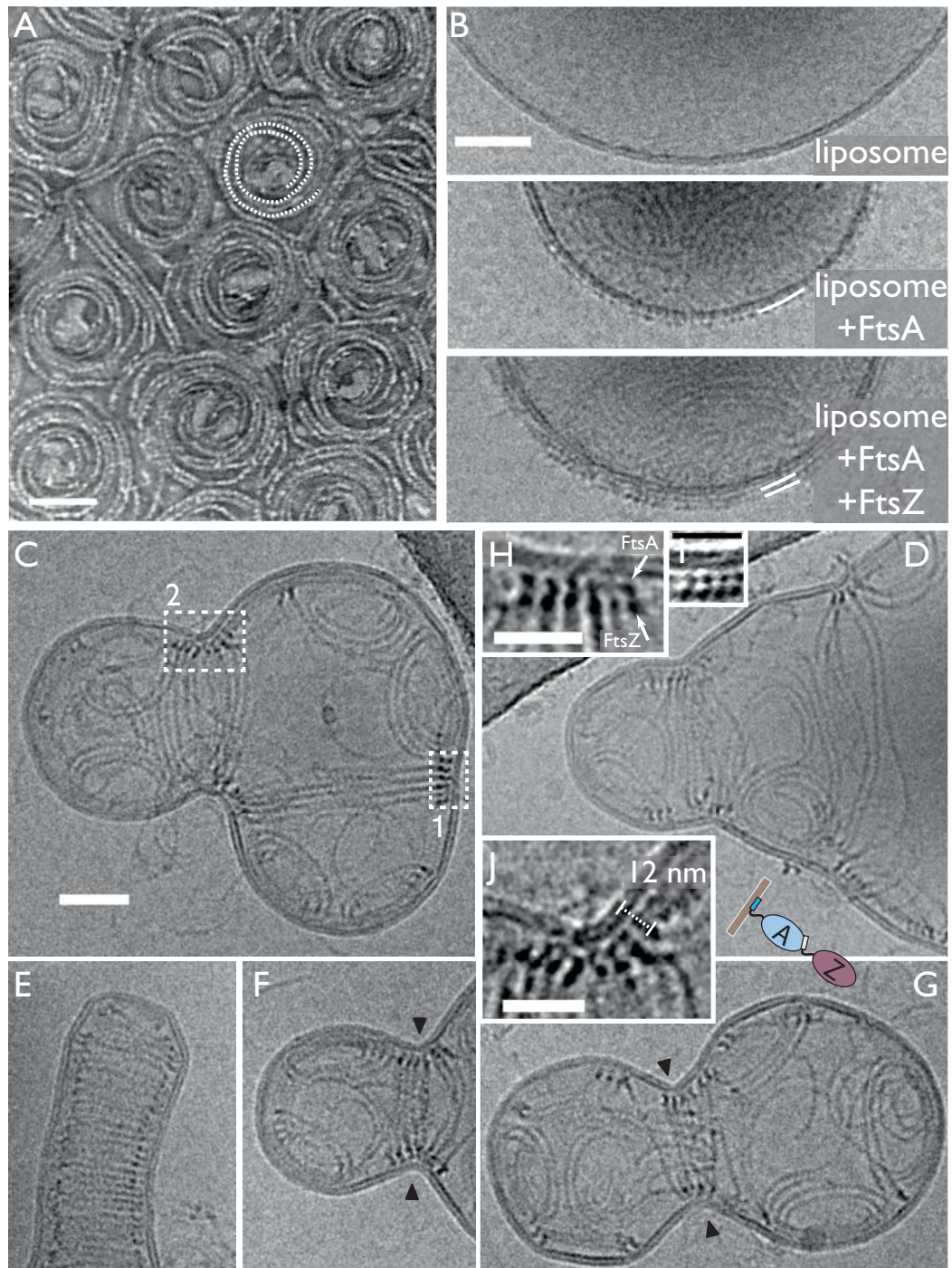


Figure 4

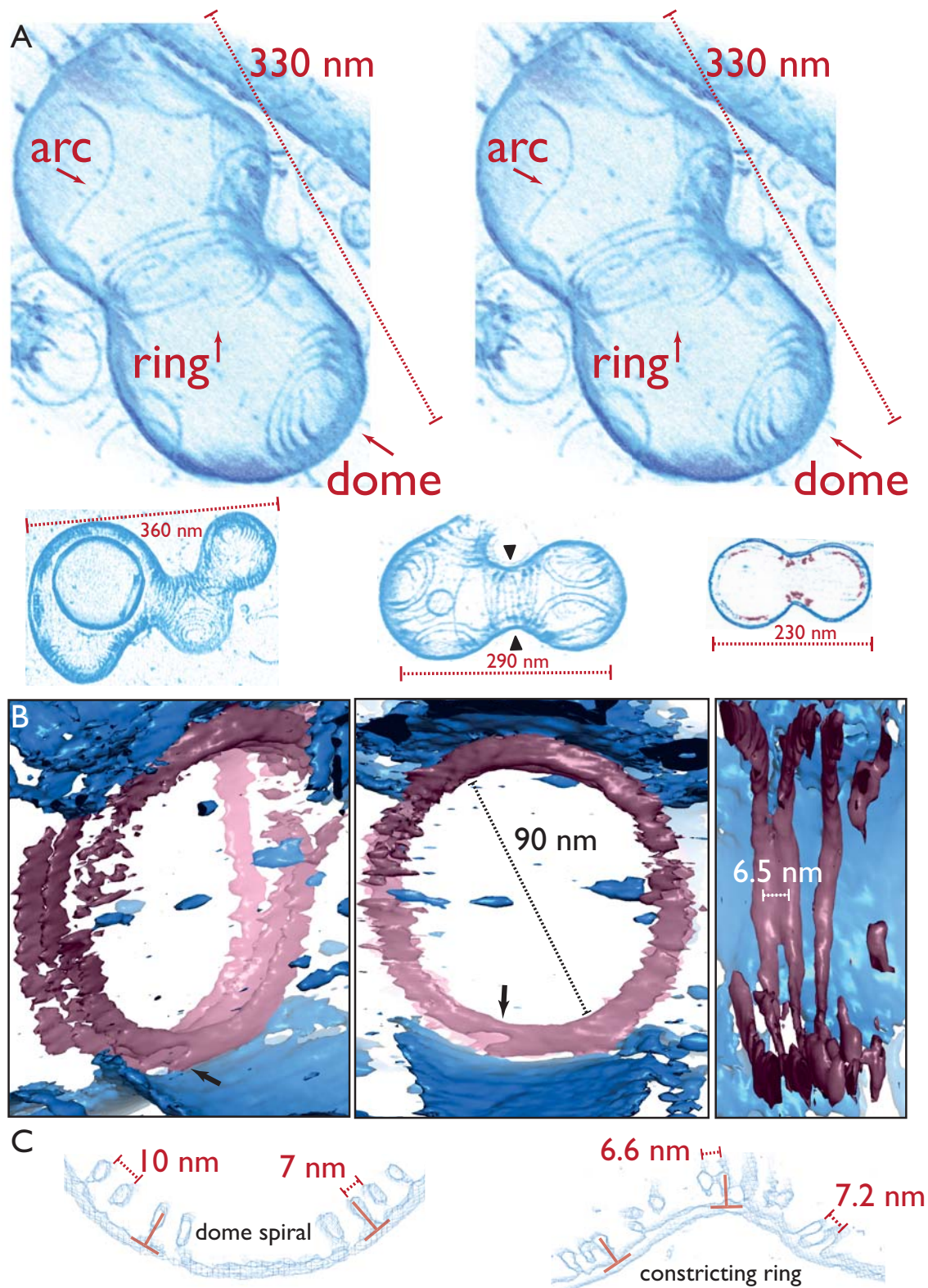


Figure 5

